Development of magnetoelastic fingering patterns in a rectangular Hele-Shaw cell

Írio M. Coutinho* and José A. Miranda†
Departamento de Física, Universidade Federal de Pernambuco, Recife, PE 50670-901 Brazil

(Received 31 March 2020; accepted 26 August 2020; published 8 September 2020)

We study the occurrence of a magnetoelastic fingering instability when a viscous ferrofluid is displaced by a nonmagnetic fluid of negligible viscosity in a horizontal, rectangular Hele-Shaw cell. Interfacial disturbances result from the interplay of viscous, elastic, and magnetic effects when the system is subjected to a uniform magnetic field, applied in the plane of the cell, and perpendicular to the initially flat interface separating the fluids. We approach the problem perturbatively through a third-order mode-coupling theory and investigate the development of interfacial patterns at early nonlinear stages of the flow. A representative collection of possible magnetoelastic fingering structures is presented which differ significantly from the classical Saffman-Taylor fingers that arise in such a rectangular cell setup in the absence of magnetic and elastic effects.

DOI: 10.1103/PhysRevFluids.5.094002

I. INTRODUCTION

Viscous fingering is an interfacial instability that occurs during the displacement of a viscous fluid by a less viscous fluid in a spatially confined environment. In their original experiments, Saffman and Taylor [1] used a rectangular channel (a rectangular Hele-Shaw cell) consisting of two horizontal, narrowly spaced, parallel glass plates. Initially, the cell is filled with a viscous oil, and then air is injected between the plates. At the beginning of the flow process, small undulations on the fluid-fluid interface are observed. Subsequently, these disturbances are amplified to fingers that penetrate into the viscous fluid. Under such conditions, the dynamic competition among the fingers eventually leads to the formation of a single smooth finger having a rounded tip. Notice that in this traditional setup of the original Saffman-Taylor problem, one deals with a situation in which there is a large difference between the values of the fluid's viscosities (large viscosity contrast limit), and gravitational forces do not play a role in determining the instability of the system (the Hele-Shaw cell is horizontal).

An alternative version of the Hele-Shaw cell setup is the so-called radial Hele-Shaw cell arrangement [2] in which a small hole is drilled through the top or bottom plate to allow the injection of fluid between the plates. In this situation, an initially circular interface turns into a deformed structure, where radially growing fingers evolve. In contrast to the rectangular cell case, these fingers are not smooth but tend to bifurcate at their tips via a tip-splitting process, creating complex branched patterns. Note that in both geometries the fingering patterns result from the interplay of viscous, pressure gradient, and surface tension effects.

A great deal of research has been done on the study of these patterns in rectangular and radial Hele-Shaw geometries. Viscous fingering belongs to a larger class of problems involving Laplacian growth, and since its discovery it has become a paradigmatic system in the area of interfacial pattern

*iriomenezes@gmail.com
†jme@df.ufpe.br

formation. For a survey of different experimental and theoretical developments on viscous fingering, see, for instance, the review articles listed in Ref. [3].

Since the seminal work by Saffman and Taylor [1], there have been many variations on the viscous fingering problem. Our current work is motivated by two particularly interesting modifications of their traditional problem in rectangular Hele-Shaw cells. The first modification, related to elastic fingering phenomena [4], introduces the action of elastic forces on the fluid-fluid interface. The second one adds the effect of magnetic forces into the fingering problem, by assuming that the displaced viscous liquid is a magnetic fluid (a ferrofluid) [5,6] and that the system is subjected to an external magnetic field. Our aim is to examine how the combined action of elastic and magnetic forces (in addition to the already participating physical effects connected to viscous forces, and pressure gradients) affects the linear stability, as well as the shape of the rising interfacial patterns at the onset of nonlinear effects. Below, we briefly present some key issues pertaining to the general behavior of elastic and magnetic field effects in existing Hele-Shaw studies. Then we lay out more specific aspects of our proposed interfacial instability problem in rectangular Hele-Shaw cell geometry, where these elastic and magnetic effects can act simultaneously.

First, let us discuss what has been known as the elastic fingering phenomenon. Recently, appealing aspects of a modified viscous fingering situation have been addressed by the consideration of interfacial elastic effects in the problem. Some years ago, an experimental study was carried out by Podgorski *et al.* [4]. They performed experiments in both radial and rectangular flow geometries to explore the possibility of creating fingering patterns on the interface separating fluids of equal viscosities. The peculiar nature of their system relies on the fact that, when the fluids are brought into contact, a chemical reaction occurs, and as a result the fluidâfluid interface becomes a thin gellike, elastic layer. Their experiments have shown that, regardless of the fluids having the same viscosities, the produced elastic interface turned out to be unstable, leading to the formation of a number of unusual patterned morphologies. In radial geometry, instead of the traditional tip-splitting patterns, unexpected mushroom-like and tentaclelike fingered structures arise. Meanwhile, in rectangular geometry, the traditional Saffman-Taylor finger having a rounded tip is replaced by a finger presenting a different feature: a flattened tip, perpendicular to the direction of motion. In conclusion, it has been verified that the existence of an elastic interface separating the fluids had a strong impact on the dynamics and morphology of the emerging interfacial patterns.

The experimental elastic fingering results reported in Ref. [4] inspired some theoretical investigations on this exciting research topic. By modeling the interface separating the fluids as a thin elastic membrane having a curvature-dependent bending rigidity, He and Belmonte [7] performed a linear stability analysis of the problem in a radial Hele-Shaw cell. They have examined both the viscosity-matched case addressed in Ref. [4], as well as the traditional maximum viscosity difference situation studied in the usual (nonelastic) Saffman-Taylor problem [1,2], where a fluid of negligible viscosity displaces a fluid of finite viscosity. Their linear results have been able to account for the fact that the reactive system is more unstable than the nonreactive one, so that reaction has a destabilizing effect. They have also shown that the elastic interface can become unstable even if the fluids have the same viscosity, consistent with the experimental findings of Ref. [4]. In addition, weakly nonlinear analysis [8] and sophisticated boundary integral numerical simulations [9] have tackled various issues related to the morphology of the elastic fingering patterns that emerge in radial geometry. These investigations [8,9] used the theoretical model proposed in Ref. [7] and consider that elastic effects dominate the behavior of the interface, in such a way that surface tension forces can be neglected. The detailed justification for the neglect of surface tension effects is given in Refs. [4,7], but essentially it is justified by the fact that, as the fluids are put into contact, a chemical reaction rapidly occurs, and a thin elastic gellike layer is immediately formed between the fluids, preventing any further direct contact between them. Under such circumstances, surface tension forces can be safely neglected. Irrespective of the scientific relevance of the elastic fingering phenomena examined in Refs. [7–9], it should be emphasized that all these theoretical works focused on the radial elastic fingering situation. Curiously, the theoretical exploration of the elastic fingering phenomena in rectangular Hele-Shaw cells has been largely overlooked.

At this point, we succinctly describe some of the most salient changes that occur in the traditional viscous fingering patterns in rectangular Hele-Shaw cells when one of the fluids is a ferrofluid and an external magnetic field is applied. Ferrofluids consist of stable colloidal suspensions of magnetic nanoscale particles dispersed in a nonmagnetic carrier liquid (water, oil, etc.) [5,6]. In the absence of an applied magnetic field, a ferrofluid behaves like a regular nonmagnetic fluid. However, when an external magnetic field is applied, it tends to align the tiny magnetic moments in the ferrofluid along its direction. The interplay of hydrodynamic and magnetic forces may dramatically modify the shape of traditional fingering patterns, when a ferrofluid is confined in a Hele-Shaw cell and subjected to an applied field. For examples of various types of experimental pattern-forming ferrofluid structures in Hele-Shaw cells, we refer the reader to Refs. [10–13]. These patterns arise under the influence of various magnetic field configurations and are normally induced by the competition of magnetic, surface tension, and gravity forces.

An example of a ferrofluid system markedly consistent with the original Saffman-Taylor setup [1], i.e., in a horizontal rectangular Hele-Shaw where a nonmagnetic fluid of negligible viscosity (air) pushes a viscous ferrofluid, can be found in the experiments of Ref. [14]. For instance, by inspecting Fig. 7 in Ref. [14] one can clearly see that, under the presence of an external magnetic field applied in the plane of the cell, and normal to the initial flat air-ferrofluid interface, the resulting fingered shape is completely different from the usual finger obtained in the nonmagnetic version of the problem [1]. In this in-plane field configuration the finger becomes much sharper than the classical, nonmagnetic Saffman-Taylor finger and develops a pointy tip (a peak). A qualitatively analogous behavior, i.e., the emergence of a finger with a sharp tip, has been detected by the fully nonlinear numerical simulations of the system, as briefly reported in M. Igonin's Ph.D. thesis [15] (in particular, see Fig. 3.27 on page 143). A similar type of ferrofluid spiky structures, also activated by an in-plane magnetic field, are obtained when a more viscous and denser ferrofluid is placed below a nonmagnetic fluid in a vertical Hele-Shaw cell under gravity [16–22]. However, the arrangement of the system investigated in Refs. [16–22] is not exactly compatible with the configuration of the original Saffman-Taylor problem [1]. It is worthwhile to note that, similar to what occurred in the elastic fingering systems commented above, theoretical studies of the in-plane field ferrofluid instability in horizontal rectangular Hele-Shaw cells have also been considerably unexplored in the literature.

From the discussion presented above on the elastic [7–9] and ferrofluid [5,6,10–15] fingering patterns that emerge in horizontal, rectangular Hele-Shaw cells, it is apparent that in both systems the resulting finger shapes are very different from the one unveiled in the conventional Saffman-Taylor problem [1], where both elastic and magnetic effects are not taken into account. Based on this evidence, and stimulated by the fact that theoretical explorations of such effects in rectangular cells are scarce, we present our current study. It should also be emphasized that the majority of the existing investigations dealing with elastic fingering analyze systems composed solely of nonmagnetic fluids, for which magnetic effects are obviously not important. On the other hand, most studies of pattern formation in confined ferrofluids assume that on the fluid-fluid interface there is a surface tension (i.e., the presence of capillary forces), meaning that interfacial elastic effects are not present and can be neglected. Therefore, it seems that a study that involves the simultaneous action of both elastic and magnetic forces on the development of fingered structures in the spirit of the original Saffman-Taylor problem is still lacking. A pertinent issue to be examined in a magnetoelastic fingering situation (in which elastic and magnetic effects act together) would be, for instance, to find out what would be the shape of the finger tip. Would it be flat as prescribed by the elastic forces, or sharp as induced by magnetic effects? Questions like this need to be addressed.

It should be noted that the theoretical magnetoelastic problem we study in this work can be connected to some real applications involving the interplay of fluid dynamic, magnetic, and elastic forces. In fact, investigators [23–28] have examined the occurrence of interfacial instabilities when ferrofluid-filled, elastic membrane systems like capsules and vesicles are under the influence of externally applied magnetic fields. A particularly interesting experimental work have been carried out in Ref. [23], where a magnetic field has been used to manipulate the shape of vesicles filled

with a ferrofluid. It has been found [23] that the applied magnetic field tends to elongate the elastic vesicle along the field's direction, making its morphology change from nearly spherical to a prolate shape. Computer simulations as well as analytical calculations more recently performed in Ref. [24] have also detected the formation of prolate spheroids at small and moderate magnetic fields, whereas elongated shapes having cusped tips have been observed at high magnetic fields. The basic techniques developed in the studies of closed elastic structures filled with ferrofluid subjected to external fields [23,24] and the encapsulation of magnetic fluids in elastic shells examined in Ref. [25] have been utilized as helpful tools to allow magnetic shape control of giant magnetoliposomes [26]. Moreover, these techniques are also utilized to probe mechanical and rheological properties of certain biological materials such as developing tissues [27] and living cells [28]. These more practical and interdisciplinary examples of soft matter, biomedical, and fluid mechanical systems involving the interaction of magnetic, hydrodynamic, and elastic effects support the academic relevance and possible practical usefulness of studies like the one we present in this work.

In this paper, we execute a linear and weakly nonlinear analysis of the magnetoelastic fingering problem in a horizontal, rectangular Hele-Shaw cell. This is done by taking into consideration both the absence and the presence of a uniform magnetic field applied in the plane of the cell. In this framework, our focus is to gain useful insights into the influence of elastic and magnetic effects on the emerging interfacial patterns, during the early nonlinear stages of the dynamics.

Before closing this section, we discuss how our current paper differs from other recent works of our research group dealing with the flow of elastic ferrofluids in Hele-Shaw cells. In Ref. [29] Livera *et al.* studied the second-order nonlinear dynamics of a confined magnetic fluid droplet (either a ferrofluid or a magnetorheological fluid) having an elastic boundary and subjected to an in-plane, *nonuniform* radial magnetic field. In contrast to our current problem, which involves a *uniform* applied magnetic field, in Ref. [29] the radial magnetic field increases linearly with the radial distance. It turns out that the presence of such a field nonuniformity introduces a huge difference between these two ferrohydrodynamic problems. When a ferrofluid sample is subjected to an externally applied magnetic field, the local magnetic field acting on the sample can include contributions from the applied field, as well as the demagnetizing field in the polarized ferrofluid. It is well known that the existence of a gradient in the local magnetic field is a key ingredient for producing a nonzero magnetic body force in a ferrofluid [5,6]. The theoretical description of such demagnetizing effects is in general quite involved and usually not amenable to analytical treatment. The particularly simple radially applied magnetic field used in Ref. [29] naturally offers a nonzero magnetic field gradient, which is not produced by complicated demagnetizing effects. On the other hand, the uniformly applied field used in this work, and in Ref. [22], has a zero gradient, and one cannot avoid dealing with intricate demagnetizing effects. In this sense, the uniform magnetic field configuration studied here and in Ref. [22] is much harder to handle analytically. Another noteworthy difference between the work performed in Ref. [29] and here is the fact that while in Ref. [29] interesting results can be extracted by a second-order perturbation theory, in this work and in Ref. [22] one has to go at least third order to have access to more stimulating nonlinear effects. In terms of differences between the physical results obtained in Ref. [29] and in this work, the most important one can be described as follows. Generally speaking, the magnetoelastic pattern-forming effects detected in Ref. [29] mostly rely on the so-called curvature weakening effect originally proposed in Ref. [7]. This effect makes fingering structures arise and protrude more easily in regions of lower bending rigidity. However, this is not exactly true in this work. For the magnetic-field-driven instability we study here, not only the bending rigidity, but also the demagnetizing field effects, are shape-dependent. Therefore, the magnetoelastic responses in our current system cannot be solely explained by weakening curvature effects. In this sense, our present magnetoelastic problem is richer than the one we studied in Ref. [29].

As mentioned earlier in this section, our current problem introduces a magnetoelastic analog of the original Saffman-Taylor problem setup [1]. For consistency with their problem, we consider flow induced by an external flow velocity, in a *horizontal* Hele-Shaw cell (for which gravitational

effects can be neglected), in which a nonmagnetic fluid of negligible viscosity displaces a viscous ferrofluid subjected to an in-plane uniform magnetic field. In a recent paper [22], we have examined a closely related physical situation involving the emergence of fingering patterns in a *vertical* rectangular Hele-Shaw cell containing a more viscous and denser, elastic interface ferrofluid placed below a nonmagnetic fluid. The system we analyzed in Ref. [22] was under the influence of both gravity and in-plane magnetic field (identical to the one used in this work), and interface deformations take place in the absence of an external flow velocity. In Ref. [22] we have also used a third-order mode-coupling theory to obtain useful information on the shape of the resulting magnetoelastic structures. These are the most important similarities and differences between the pattern formation problems studied here and in Ref. [22]. At first glance, it may appear that our magnetoelastic investigations carried out here for a horizontal Hele-Shaw cell, and in Ref. [22] for a vertical Hele-Shaw cell, are too similar physically and as a result should lead to exactly identical pattern-forming shapes and dynamical behaviors. Nevertheless, this is not necessarily true. In the midst of all this, it should be clear that a common feature to both magnetoelastic problems we study (i.e., in horizontal and vertical setups) is the fact that the systems evolve dynamically up to nonlinear stages. Therefore, one cannot *a priori* determine the weakly nonlinear behavior of the system we examine in this work, based on the existing information of the system we studied in Ref. [22]. This is in fact what justifies the work performed by experimentalists while investigating the development of confined, nonelastic ferrofluid peak patterns under the very same in-plane magnetic field configurations examined here and in Ref. [22]: in Ref. [14] they analyzed the problem in a horizontal Hele-Shaw cell, and in Ref. [17] they examined the equivalent problem in a vertical Hele-Shaw cell. Their experimental results revealed the development of ferrofluid peak structures arising in both Hele-Shaw cell arrangements, but the details of the resulting shapes could eventually differ depending on whether they emerge in horizontal or vertical cells. Likewise, several different research groups have investigated seemingly identical situations in both horizontal and vertical rectangular Hele-Shaw cell setups for the study of viscous fingering with nonmagnetic fluids [3]. For all these reasons, we believe the investigation performed in this work is fully justified. In the end, as discussed in Sec. III C, we will show that some of the magnetoelastic pattern-forming structures found here have not been detected in Ref. [22]. An example of such structures are the ones we have obtained under the absence of external magnetic field, a situation that could not have been explored in Ref. [22], since in a vertical cell the corresponding interface is flat and stable. Another interesting pattern-forming structure that is unique to the horizontal cell case, and obtained at low magnetic field intensities, is the magnetoelastic finger that presents a peculiar straight front. Moreover, contrary to what has been done in Ref. [22], in this work we also exploited possible weakly nonlinear, third-order shapes emerging when the elastic forces are replaced by surface tension at the interface separating the fluids (Sec. III C 1 and the Appendix), finding good qualitative agreement with the associated patterns obtained by experiments [14] and fully nonlinear numerical simulations [15]. These horizontal Hele-Shaw cell findings allow one to gain useful insights into the morphology of still unexplored magnetoelastic patterns in the rectangular flow setup.

II. GOVERNING EQUATIONS AND THE MODE-COUPLING APPROACH

Consider a horizontal Hele-Shaw cell of thickness b containing two semi-infinite immiscible viscous fluids. The viscosities of the displacing and displaced fluids are denoted, respectively, as η_1, and η_2, and the cell lies on the xy plane (see Fig. 1). The displacing fluid is injected at constant external flow velocity $\mathbf{v}_\infty$ at $y = -\infty$, and the displaced fluid is withdrawn at the same velocity at $y = +\infty$. We describe the problem in a frame moving with velocity $\mathbf{v}_\infty$ so that the interface may deform, but it does not displace from $y = 0$ on average. The displacing fluid is nonmagnetic (zero magnetization), and the displaced fluid is a ferrofluid having a magnetization $\mathbf{M}$. A uniform external magnetic field

$$\mathbf{H}_0 = H_0\hat{\mathbf{y}} \tag{1}$$

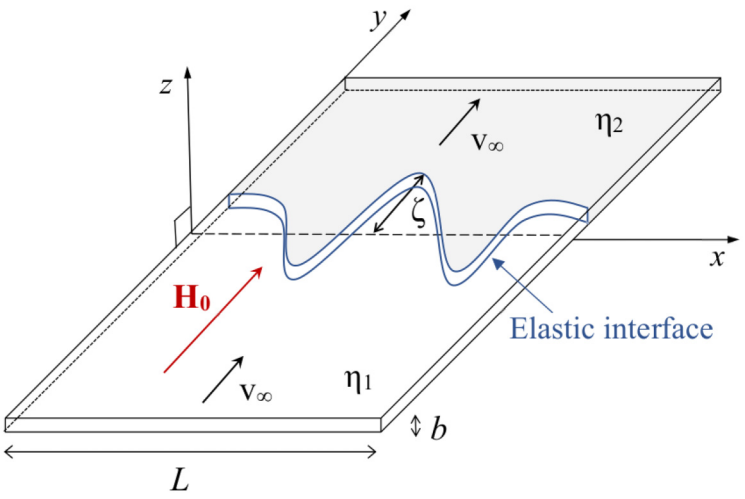

FIG. 1. Schematic representation of the magnetoelastic fingering problem in a horizontal, rectangular Hele-Shaw cell of thickness b. Fluid 1 is nonmagnetic and has viscosity η_1, while fluid 2 is a ferrofluid (in gray) of viscosity η_2 (where $\eta_2 \gg \eta_1$). The constant external flow velocity is given by $\mathbf{v}_\infty$. The interface separating the fluids is elastic and has a curvature-dependent bending rigidity given by ν [see Eq. (8)]. A uniform magnetic field $\mathbf{H}_0$ is applied in the plane of the cell (x-y plane), pointing along the positive y direction. The initially unperturbed interface lies along $y = 0$, and interfacial perturbations are represented by $y = \zeta = \zeta(x, t)$, where $0 \leqslant x \leqslant L$.

is applied in the plane of the cell, being normal to the initially flat boundary that separates the fluids. In Eq. (1) $\hat{\mathbf{y}}$ represents the unit vector along the y direction. For the sake of generality, we perform our calculations considering the situation in which there is a general viscosity contrast between the fluids. However, we focus on the classical Saffman-Taylor situation, which has been largely explored both theoretically and experimentally in rectangular Hele-Shaw flows [1,3,14], where the viscosity of the displacing fluid is negligible compared with the viscosity of the displaced one.

For the quasi-two-dimensional geometry of the rectangular Hele-Shaw cell involving ferrofluids, our fluid dynamics problem is described by a modified Darcy's law for the gap-averaged velocity [5,6]

$$\mathbf{v}_j + \mathbf{v}_\infty = -\frac{b^2}{12\eta_j}\left\{\nabla p_j - \frac{1}{b}\int_{-b/2}^{+b/2} \mu_0(\mathbf{M}\cdot\nabla)\mathbf{H}\, dz\right\}, \tag{2}$$

where $j = 1$ ($j = 2$) labels the displacing (displaced) fluid, $\mathbf{v}_j$ is a velocity field, p_j denotes the pressure, and μ_0 is the free-space magnetic permeability. In Eq. (2) it should be noted that $|\mathbf{M}| = M = 0$ for the nonmagnetic fluid. Here we follow the standard approximations used by other investigators [5,6,10–14] and assume that the ferrofluid is magnetized such that its magnetization is constant and collinear with the applied field $\mathbf{M}(\mathbf{H}) = M(H_0)\hat{\mathbf{y}}$. Therefore, we include just the lowest order effect of the magnetic interactions that would result in fluid motion.

The local magnetic field appearing in Eq. (2) differs from the applied field $\mathbf{H}_0$ [Eq. (1)] by a demagnetizing field of the polarized ferrofluid

$$\mathbf{H} = \mathbf{H}_0 + \mathbf{H}_d, \tag{3}$$

where $\mathbf{H}_d = -\nabla\varphi$, and φ is a scalar magnetic potential. Notice that since in this work the applied field is spatially uniform, it eventually drops out in the calculation of the magnetic term in Eq. (2), and the magnetic effects are entirely due to the demagnetizing field. Inasmuch as $\mathbf{H}_0$ has a zero gradient, the complicated demagnetizing field contribution must be taken into account since it is

the first nonzero correction to the magnetic body force. In fact, the demagnetizing effects play an important role in the emergence of the magnetoelastic peak patterns we study in this work.

It is convenient to rewrite Eq. (2) in terms of velocity potentials because the velocity field $\mathbf{v}_j$ is irrotational. Since we are interested in perturbations of the velocity field around a steady flow, we write $\mathbf{v}_j = -\mathbf{v}_\infty - \nabla\phi_j$ where ϕ_j defines a velocity potential. Both sides of Eq. (2) are recognized as gradients of scalar fields. Integrating both sides of Eq. (2) yields

$$\phi_j = \frac{b^2}{12\eta_j}\left\{p_j + \mu_0\frac{M}{b}\int_{-b/2}^{+b/2}\frac{\partial\varphi}{\partial y}dz\right\} + \eta_j v_\infty y \tag{4}$$

after dropping an arbitrary constant of integration. For the geometry of our problem the magnetic potential appearing in Eq. (4) is written as

$$\varphi = \frac{1}{4\pi}\int_{\mathcal{S}}\frac{\mathbf{M}\cdot\mathbf{n}'}{|\mathbf{r}-\mathbf{r}'|}d^2r' = \frac{1}{4\pi}\int_{-\infty}^{+\infty}\int_{-b/2}^{+b/2}\frac{M\hat{\mathbf{y}}\cdot\mathbf{n}'\,dx'\,dz'}{\sqrt{(x-x')^2+(y-y')^2+(z-z')^2}}, \tag{5}$$

where the z axis points along the direction transverse to the plates of the cell. In Eq. (5) the unprimed coordinates $\mathbf{r}$ denote arbitrary points in space, the primed coordinates $\mathbf{r}'$ are integration variables within the magnetic domain $\mathcal{S}$, and $d^2r' = dx'\,dz'$ represents the infinitesimal area element. The vector $\mathbf{n}'$ represents the unit normal to the magnetic domain in consideration. Note that from Eq. (4), and the incompressibility condition $\nabla\cdot\mathbf{v}_j = 0$, it can be verified that the velocity potentials obey Laplace's equation. Therefore, the velocity potentials can be written as

$$\phi_j = \sum_{k\neq 0}\phi_{jk}(t)e^{(-1)^{j-1}|k|y}e^{ikx}. \tag{6}$$

Observe that in obtaining these potentials we assume that, for points far from the interface, we expect uniform, steady flow uninfluenced by the interface. So we require that the system evolves with uniform velocity $\mathbf{v}_\infty$ in the limits $y \to \pm\infty$. Recall that $\mathbf{v}_j$ are measured in the comoving frame and thus vanish at these limits. Therefore, the velocity potentials ϕ_j given in Eq. (6) go to constants (that we set to zero) as $y \to \pm\infty$. It is also clear that these potentials obey periodic boundary conditions along the x axis.

By subtracting Eq. (4) for one fluid from the same equation for the other fluid, and then dividing the resulting expression by the sum of the two fluids' viscosities, we obtain

$$A\left(\frac{\phi_1+\phi_2}{2}\right) - \left(\frac{\phi_1-\phi_2}{2}\right) = -\frac{b^2}{12(\eta_1+\eta_2)}\left[(p_1-p_2) + \mu_0\frac{M^2}{b}\varphi\right] + Av_\infty y, \tag{7}$$

which is a basic equation of motion of our problem expressing the discontinuity of velocity potentials at the two-fluid interface. On the right-hand side of Eq. (7), $p_1 - p_2$ is the pressure jump across the interface. On the other hand, on the left-hand side of Eq. (7) $A = (\eta_2 - \eta_1)/(\eta_2 + \eta_1)$ stands for the viscosity contrast, which in our case of interest is equal to one.

As commented in Sec. I, in addition of considering that the displacing fluid is a ferrofluid, we also assume that the boundary separating the fluids is elastic. Concerning the elastic properties of the interface, we follow Ref. [7] and consider that the interface separating the fluids is a thin elastic membrane presenting a curvature-dependent bending rigidity given by

$$\nu = \nu(\kappa) = \nu_0[Ce^{-\lambda^2\kappa^2} + 1 - C], \tag{8}$$

where

$$\kappa = \left(\frac{\partial^2 y}{\partial x^2}\right)\left[1 + \left(\frac{\partial y}{\partial x}\right)^2\right]^{-\frac{3}{2}} \tag{9}$$

represents the local interfacial curvature in the plane of the Hele-Shaw cell. This model is based on the fact that interface deformations tend to decrease the rigidity. Therefore, $\nu(\kappa)$ should decrease

as κ is increased. In Eq. (8) ν_0 is the maximum rigidity that expresses the largest resistance to disturbances, and $0 \leqslant C < 1$ is the bending rigidity fraction, which measures the fraction of intramolecular bonds broken through surface deformation. Moreover, $\lambda > 0$ denotes a characteristic length beyond which $\nu(\kappa)$ decreases substantially.

In order to bolster the practical relevance of our theoretical study, and to make reference to possible experimental realizations of our magnetoelastic problem, we stress that we consider that the elastic, gellike ferrofluid interface we model is originated by a chemical reaction as in the case already studied experimentally [4] and theoretically [7–9] for nonmagnetic fluid flows in Hele-Shaw cells. We emphasize that, even though there are a couple of recent theoretical studies on elastic interface ferrofluids in radial [29,30] and rectangular [22] Hele-Shaw cells, to the best our knowledge there are no existing experimental realizations of such magnetoelastic phenomena in Hele-Shaw flows. Nevertheless, in principle, this is no practical impediment in combining ferrofluids with micellar systems if, for instance, one mixes the magnetic colloids with one of the solutions used in Ref. [4] (or another surfactant/salt couple) [31]. But one has to take care about orders of magnitudes of the viscoelastic properties of the micellar gel that forms at the interface, and the forces that arise from ferrofluid, so that one is not negligible compared to the other. Also, for micellar systems, the fluids must be water based [31], so one should use a water-based ferrofluid [5,6,10–13]. As a displacing fluid of negligible viscosity one could use a dilute, water-based "white spirit" (an organic liquid), which usually has viscosity orders of magnitude lower than ferrofluids (see, for example, Refs. [17,32]).

Due to the interplay of magnetic, viscous, and elastic forces, the interface separating the fluids may deform, and its perturbed shape is described as

$$y = \zeta(x,t) = \sum_{k=-\infty}^{+\infty} \zeta_k(t) \exp(ikx), \tag{10}$$

where

$$\zeta_k(t) = \frac{1}{L} \int \zeta(x,t) \exp(-ikx)\, dx \tag{11}$$

denotes the complex Fourier mode amplitudes with wave numbers k, and $0 \leqslant x \leqslant L$. Equation (10) includes all possible modes k, with the exception of $k = 0$ since we are in the comoving frame. The wave vectors can be either positive or negative and are constrained to lie on the x axis. We apply periodic boundary conditions along the x axis, limiting the values of the wave number to discrete allowed values $2\pi n/L$, for integer n.

In this work, we pay closer attention to the intermediate dynamic stage that bridges the initial, purely linear [i.e., $O(\zeta_k)$], and the fully nonlinear, late-time regimes of the interface evolution. A great deal of research has been done on the advanced time stages of rectangular Hele-Shaw flows, namely, on the development of steady state fingers and on the selection of finger widths [1,3]. However, in this work we focus on the analysis of the weakly nonlinear time-dependent stages of the flow and will not directly address these well-studied steady state structures. To do that, we use a perturbative weakly nonlinear approach and keep terms up to third order in ζ [$O(\zeta_k^3)$]. We underscore that the incorporation of such relatively high-order perturbative terms is essential to properly capture and describe the underlying magnetoelastic fingering process and related morphological aspects of the interface. From this point onwards, our main goal is to derive a mode-coupling differential equation that describes the time evolution of the interfacial amplitudes $\zeta_k(t)$. To get such a differential equation for $\zeta_k(t)$, we have to deal with the relevant boundary conditions of the problem.

The first boundary condition gives the pressure jump across the perturbed interface $y = \zeta$ [7–9]:

$$(p_1 - p_2)|_{y=\zeta} = \frac{1}{2}\nu'''\kappa^2\kappa_s^2 + \nu''\left(3\kappa\kappa_s^2 + \frac{1}{2}\kappa^2\kappa_{ss}\right) + \nu'\left(\frac{1}{2}\kappa^4 + 3\kappa_s^2 + 2\kappa\kappa_{ss}\right) + \nu\left(\frac{1}{2}\kappa^3 + \kappa_{ss}\right) - \frac{1}{2}\mu_0(\mathbf{M}\cdot\mathbf{n})^2. \tag{12}$$

In Eq. (12) the primes indicate derivatives with respect to the curvature κ, while the subscripts of κ indicate derivatives with respect to the arclength s. Note that Eq. (12) differs significantly from the traditional Young-Laplace condition applied to immiscible nonreactive fluids in Hele-Shaw cells [1,3] that is much simpler and involves only the product of the curvature κ by the surface tension σ. Similarly to what is done in Refs. [7–9], we consider that elastic effects dominate the condition at the interface, in such a way that the surface tension effects are not considered in Eq. (12). Notice that within the framework of our study, and consistent with Refs. [4,7–9], the effects of the chemical reaction are fully taken into account by the consideration of the nontrivial pressure jump boundary condition given in Eq. (12). In other words, it is through Eq. (12) that the effects of the chemical reaction associated with our elastic fingering problem are incorporated into the derivation of our mode-coupling differential equation for $\zeta_k(t)$ [Eq. (14)].

Note that Eq. (12) also includes a contribution coming for the magnetic nature of the displaced fluid. The last term on the right-hand side of Eq. (12), which is commonly known as the magnetic normal traction term [5,6], takes into account the influence of the discontinuous normal component of the magnetization at the interface. This magnetic piece produces terms associated only with even powers of ζ, so it is at least of second order in the interface perturbation. In spite of this, the magnetic traction term will also have a role in determining the overall shape of the emerging magnetoelastic patterns when nonlinear effects take over.

The problem is then fully specified with the consideration of a second relevant boundary condition, the so-called kinematic boundary condition, which states that the normal components of each fluid's velocity are continuous at the interface [1,3,5,33,34]:

$$\mathbf{n}\cdot\nabla\phi_1 = \mathbf{n}\cdot\nabla\phi_2. \tag{13}$$

This condition holds for either fluid-fluid, fluid-elastic, or fluid-solid interfaces and states that the fluid cannot penetrate into the other medium. In our case, the problem effectively involves three immiscible phases (the two liquids and the elastic interface). Nonetheless, since the elastic phase has negligible thickness (and thus cannot be compressed in the normal direction), the normal component of the fluid velocity must be continuous across the interface.

At this point we have all ingredients to get a mode-coupling differential equation that describes the time evolution of the interfacial amplitudes $\zeta_k(t)$. We proceed by using boundary conditions (12) and (13) to express ϕ_j [Eq. (6)] in terms of ζ_k [Eq. (10)] consistently up to third order. Then, by substituting these relations in Eq. (7), and Fourier transforming, this yields a *dimensionless* mode-coupling equation for the system (for $k \neq 0$):

$$\begin{aligned}\dot{\zeta}_k = {} & \Lambda(k)\,\zeta_k + \sum_{q\neq 0}\{F(k,q)\,\zeta_q\zeta_{k-q} + G(k,q)\,\dot{\zeta}_q\zeta_{k-q}\} \\ & + \sum_{p,q\neq 0}\{H(k,p,q)\,\dot{\zeta}_p\zeta_{q-p}\zeta_{k-q} + I(k,p,q)\,\dot{\zeta}_p\zeta_q\zeta_{k-p-q} \\ & + [J(k,p,q) + K(k,p,q)]\,\zeta_p\zeta_q\zeta_{k-p-q}\},\end{aligned} \tag{14}$$

where the overdot represents a total time derivative, and

$$\Lambda(k) = |k|[N_B W_1(k) + AU - k^4] \tag{15}$$

denotes the linear growth rate. The parameter

$$N_B = \frac{\mu_0 M^2 b^3}{\nu_0} \tag{16}$$

represents a magnetoelastic number and measures the ratio of magnetic to elastic forces. The magnetic integral

$$W_1(k) = \frac{1}{4\pi}\int_{-\infty}^{\infty}(1-e^{ik\tau})\left\{\frac{2}{\tau^2}[\sqrt{1+\tau^2}-|\tau|]\right\}d\tau, \tag{17}$$

is a positive quantity [$W_1(k) > 0$], being the first-order contribution from the demagnetizing field. In addition

$$U = \frac{12(\eta_2 + \eta_1)b^2 v_\infty}{\nu_0} \tag{18}$$

defines a characteristic velocity and measures the importance of viscous effects relative to the elastic ones.

At second order, the mode-coupling terms are given by

$$F(k, q) = \frac{N_B}{2}|k|q(k - q) \tag{19}$$

and

$$G(k, q) = A|k|[1 - \mathrm{sgn}(kq)], \tag{20}$$

with the sign function sgn being equal to ± 1 according to the sign of its argument. The coupling term (19) comes from magnetic normal traction contribution in the pressure jump condition (12). Moreover, the nonlinear term given by Eq. (20) originates from the coupling of the perturbed flow $\dot{\zeta}$ with the interface shape perturbation ζ. Note that there is no demagnetizing field contribution at second order.

Finally, the third-order mode-coupling terms are

$$H(k, p, q) = |k||q|\mathrm{sgn}(pq)[1 - \mathrm{sgn}(kq)], \tag{21}$$

$$I(k, p, q) = p\left[k - q - \frac{p}{2} - \frac{|k||p|}{2p}\right], \tag{22}$$

$$J(k, p, q) = |k|(k - p - q)^2\left[C\lambda^2 p^2 q^3(12p + 6q) - \frac{5}{2}(k - p - q)^2 pq - 10p^3 q - \frac{5}{2}p^2 q^2\right]. \tag{23}$$

Similar to what occurred in second order, the third-order terms given in Eqs. (21) and (22) result from the coupling of the perturbed flow with the perturbed interface shape. Nonetheless, it is worth pointing out that the coupling term (23) is the only term in the entire equation of motion (14) that contains a contribution from the bending rigidity fraction C. This particular third-order term is of importance to evaluate the role of the curvature-dependent bending rigidity [Eq. (8)] in determining the nature and intensity of the finger peak instability that may arise in our problem. The last third-order mode-coupling term is given by

$$K(k, p, q) = N_B|k|\left[\frac{3}{2}W_2(k - p - q, p, q) - \frac{pq}{2}W_3(k - p - q, p, q)\right], \tag{24}$$

where the magnetic integrals

$$W_2(k, p, q) = \frac{1}{4\pi}\int_{-\infty}^{\infty}[(e^{ik\tau} - 1)(e^{ip\tau} - 1)(e^{iq\tau} - 1)]\left\{\frac{2}{3\tau^2}\left[\frac{2\sqrt{1+\tau^2} - |\tau|}{\tau^2} - \frac{1}{\sqrt{1+\tau^2}}\right]\right\}d\tau \tag{25}$$

and

$$W_3(k, p, q) = \frac{1}{4\pi}\int_{-\infty}^{\infty}[(e^{ik\tau} - 1)e^{ip\tau}e^{iq\tau}]\left\{\frac{2}{\tau^2}[\sqrt{1 + \tau^2} - |\tau|]\right\}d\tau \tag{26}$$

express the third-order contributions from the demagnetizing field.

It should be stressed that in Eqs. (14)–(26) lengths and velocities are rescaled by b and $\nu_0/[12(\eta_1 + \eta_2)b^2]$, respectively. Recall that we focus on the situation in which $\eta_2 \gg \eta_1$, so that $A = 1$. This is done to allow some connection with existing experiments reported in Refs. [1,3,5,6,14]

and with numerical simulations [15], where ferrofluid patterns arise in the absence of elastic effects. For a detailed study of the role of the viscosity contrast in determining the dynamics of the interface for a rectangular Hele-Shaw case in which magnetic and elastic effects are not considered, see Ref. [35]. Note that the theoretical results presented in this work utilize dimensionless quantities which are consistent with physical parameters used in Refs. [4,7–9,14,16,17,36].

Equation (14) is the third-order mode-coupling equation of the magnetoelastic problem in a horizontal rectangular Hele-Shaw cell. A similar set of equations have been recently obtained in Ref. [22] for the equivalent problem in a vertical Hele-Shaw cell, under the action of gravitational effects, and in the absence of an externally applied velocity field. Note that while the linear growth rate $\Lambda(k)$ gives information about the linear stage of the interface dynamics, the nonlinear terms given by Eqs. (19)–(26) allow one to extract valuable information about most prominent morphological features of the patterns produced in the weakly nonlinear regime.

III. DISCUSSION

A. First order

As commented in Sec. I, there are some linear stability analyses of elastic fingering phenomena in radial Hele-Shaw cells (involving nonmagnetic [7–9], as well as magnetic fluids [29,30]). However, with the exception of our previous on vertical Hele-Shaw cells [22], corresponding studies in rectangular Hele-Shaw cells have been unexplored. So, although the main focus of our work is to study the influence of elastic and magnetic effects on the *weakly nonlinear* dynamics of the system, before proceeding to higher orders, we briefly discuss some noteworthy features of the linear regime (first-order in ζ) in rectangular flow geometry.

First order in the mode-coupling expansion reduces to usual linear stability analysis. From the first term on the right-hand side of Eq. (14), one can see that each mode grows or decays independently of all others, with exponential growth rate $\Lambda(k)$ given by Eq. (15). Positive values of $\Lambda(k)$ make a mode unstable to growth of an initially small perturbation. Keeping this in mind, and by observing the linear dispersion relation (15), it is apparent that the first term inside the square brackets ($N_B W_1(k)$) is destabilizing (i.e., demagnetizing field effects induce a positive growth rate). Likewise, the characteristic velocity U acts to destabilize the interface. On the other hand, the term proportional to k^4 which is associated with the constant bending rigidity ν_0 [Eq. (8)] is stabilizing and tends to restrain interface deformation. Therefore, at the linear level of the dynamics in rectangular Hele-Shaw cells, elasticity acts similarly to surface tension in the equivalent, nonelastic version of the problem [1,3].

Note that the relevant curvature-dependent bending rigidity parameters C and λ [Eq. (8)] are not present in the linear growth rate expression (15). This particular observation, valid for the fingering problem including an elastic interface in rectangular Hele-Shaw cells, is quite different from the corresponding scenario in *radial* Hele-Shaw cells [7–9]. In radial geometry [7–9] the linear growth rate expression is a bit more involved and presents a bending elasticity term that does depend explicitly on C and λ. It turns out that in Refs. [7–9] the presence of such parameters allows the elasticity term in the growth rate to be either negative or positive. This means that in radial geometry, and already at the linear level, depending on the values of C and λ, the bending elasticity contribution could be either stabilizing or destabilizing. This peculiar behavior revealed in the theoretical studies for the radial elastic fingering problem was essential to allow the authors of Ref. [7] to show, consistently with the experiments of Ref. [4], that the elastic interface could deform under unexpected circumstances. For example, the elastic interface could be unstable if the viscosity of the fluids are equal or even if the displacing fluid is more viscous. These findings substantiate the usefulness and validity of the curvature-dependent bending rigidity model proposed in Ref. [7], which is also employed in this work. However, as expressed by Eq. (15), this interesting effect detected for radial elastic fingering does not show up during the linear regime in the rectangular version of the problem.

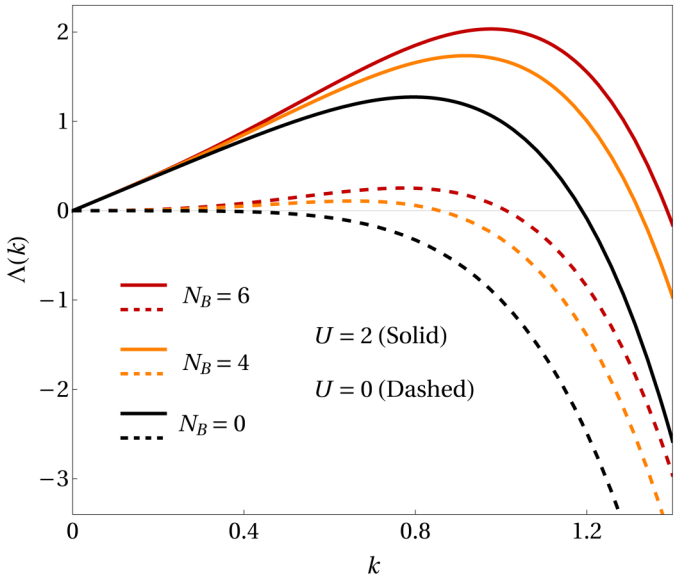

FIG. 2. Plot of the linear growth rate $\Lambda(k)$ as a function of wave number k, for three values of the magnetoelastic number N_B and two values of the characteristic velocity U.

A useful quantity that can be extracted from Eq. (15) is the wave number of maximum growth rate k^*, obtained by setting $[d\Lambda(k)/dk]_{k=k^*} = 0$. This specific value of k characterizes the dominant wave number of the emergent patterns in the linear stage. Note that due to the presence of the demagnetizing field integral $W_1(k)$ in Eq. (15), k^* cannot be easily calculated analytically. In this way, we determine k^* by solving a transcendental equation numerically. The most unstable wave number k^* will be used as the dominant (or, fundamental) mode in our mode-coupling, weakly nonlinear analysis. Another special wave number is the threshold (or, critical) wave number k_c [obtained by setting $\Lambda(k) = 0$], beyond which all modes are stable. This critical mode defines a band of linearly unstable modes.

To illustrate some of these linear stability issues a bit more quantitatively, in Fig. 2 we plot the linear growth rate $\Lambda(k)$ for three values of the magnetoelastic number N_B: 0, 4, and 6. For each value of N_B, we graph $\Lambda(k)$ for two values of the characteristic velocity: $U = 0$ (dashed curves), and $U = 2$ (solid curves). The curves in Fig. 2 display a range of wave numbers over which $\Lambda(k)$ can be positive or negative. First, look at the case in which $U = 0$ (dashed curves). Of course, when $U = 0$ and $N_B = 0$ the interface is stable, and the growth rate is negative. The in-plane magnetic field is destabilizing, while the elastic rigidity of the interface tends to stabilize short-wavelength deviations. As N_B grows, the system becomes increasingly unstable, and regions of $\Lambda(k) > 0$ arise. When $U = 2$ (solid curves), both U and N_B conspire to destabilize the system. Consequently, the fastest growing mode k^* and the critical mode k_c shift to the right. As a result, modes of higher wave number become unstable. Likewise, for any particular mode k, the linear growth rate $\Lambda(k)$ increases, causing perturbations to grow more rapidly. These findings exemplify the essential information one can get at first order. Recall that, at the linear level, one cannot identify the role played by the curvature-dependent bending rigidity (i.e., of parameters C and λ) and is unable to make any specific predictions on how the combined whole of C, λ, and N_B influence the shape of the elastic interface.

B. Second order

To analyze pattern formation processes at the onset of nonlinearities, and to examine the impact of magnetic and curvature-dependent bending rigidity effects on the morphology of the elastic

interface, we go beyond linear stability analysis. After the initial interface deformation, as the unstable modes of perturbation grow, they become coupled in a weakly nonlinear stage of evolution. It is well known that mode-coupling analysis can offer useful insights into the morphology of the growing interface during the weakly nonlinear regime in Hele-Shaw flows [35,37]. Therefore, we use such a theoretical tool to explore early nonlinear aspects of our magnetoelastic problem. Even though in Sec. I we carried out our mode-coupling calculations to third order, we systematically examine nonlinear terms in order of their strength at the onset of the instability. Therefore, we initiate our discussion on nonlinear effects by examining relevant contributions that arise at second order. Third-order contributions will be discussed in Sec. III C.

Inspecting the mode-coupling Eq. (14), and more specifically the second-order terms given in Eqs. (19) and (20), we observe that, as in the case of the linear growth rate $\Lambda(k)$ [Eq. (15)], they do not involve the curvature-dependent bending rigidity parameters parameters C and λ. In addition, there is no contribution from the important demagnetizing field effects at second order. As a consequence, and unfortunately, we simply cannot have access to the influence of such important physical effects at the second-order level.

However, the second-order mode-coupling terms $F(k, q)$ and $G(k, q)$ have a dependence on N_B, and A, respectively. Our research group has previously analyzed the role of these second-order terms in rectangular flow geometry for magnetic [20] and nonmagnetic [35] fluids. The results obtained in Refs. [20,35] remain unchanged under the circumstances of our current problem, so here we will simply highlight a few important points. First, notice that the second-order mode-coupling term $F(k, q)$ is originated from the magnetic normal traction contribution in the pressure jump condition (12). In Ref. [20], the rising of nonelastic ferrofluid peaks was analyzed by considering the coupling of modes $k = k^*$ (the fundamental mode) and $2k$ (its first harmonic). It has been shown that this nonlinear coupling forces the growth of mode $2k$ and selects a preferred phase that provokes a finger-tip-sharpening phenomenon induced by magnetic effects. In this context, it has been found that larger N_B lead to the formation of sharper ferrofluid finger tips. On the other hand, in Ref. [35] it has been shown that the viscosity contrast A acts to break the statistical up-down symmetry of the linear stability theory. Essentially, the second-order term $G(k, q)$ can accelerate growth of the subharmonic mode $k/2$, generating a finger competition process dependent upon A. Nonetheless, such a finger competition mechanism does not really affect the focus of our current work, which is essentially on understanding how the shape of a finger is impacted by magnetoelastic effects, in the traditional high-viscosity limit (i.e, for a fixed $A = 1$) [1,3].

C. Third order

In this section, we examine the whole mode-coupling equation (14), taking into account the contributions coming from the third-order terms [Eqs. (21)–(26)]. By examining these terms, the need to study our magnetoelastic, rectangular geometry problem perturbatively up to such high-orders becomes clear: a closer look at Eq. (23) shows that this particular third-order term does depend on the curvature-dependent bending rigidity terms C and λ. Furthermore, an inspection of Eq. (24) reveals that this term is composed of pieces coming from demagnetizing field effects related to the magnetic integrals W_2 and W_3 [Eqs. (25) and (26)]. Therefore, this is the lowest perturbative order at which we can investigate how curvature-dependent elastic effects come into play and act jointly with magnetic effects to influence the shape of the fingered patterns. Thus, despite the lengthy and somewhat complicated nature of Eqs. (21)–(26), it should be noted that our third-order calculation is motivated by nothing more than a practical necessity.

To investigate the development of magnetoelastic interfacial patterns in horizontal, rectangular Hele-Shaw cells at third order, we follow Refs. [20,29,35–37] and consider the nonlinear coupling of a relatively small number of Fourier modes. More specifically, in accordance with Ref. [36], we consider the coupling of just four modes: a dominant fundamental mode taken as the fastest growing mode $k = k^*$ and its three subsequent harmonic modes $2k$, $3k$, and $4k$. It is worth noting that once $k = k^*$ is the maximum of the linear growth rate, all the harmonic modes lie to the right

of the band of unstable modes defined by k_c. As a result, the harmonics are always linearly stable, and any growth of the harmonic modes is genuinely caused by weakly nonlinear effects. It has been shown [36] that the consideration of these four participating Fourier modes allows one to capture the most relevant morphological aspects of the emerging nonlinear patterns (e.g., finger-tip broadening, finger-tip sharpening, side-branching events, etc.). It has also been verified that the addition of more harmonic modes would not introduce any significant qualitative modifications in the shape or basic dynamics of the resulting fingers.

Several morphological scenarios can result from the weakly nonlinear interaction of these participating modes. Growth of the dominant fundamental mode creates a sinusoidal oscillation of the initially flat interface, forming fingers of each fluid penetrating into the region previously occupied by the other fluid. On the other hand, through mode coupling, the harmonic modes influence the ultimate shape of the emerging fingering structures. For example, favored growth of mode $2k$ may determine if the fingers are sharp or wide, inducing finger-sharpening or finger-broadening behaviors [35,37]. Preferred growth of mode $3k$ may dictate whether fingers develop protuberances near their tips connected to side-branching phenomena (front lobe accompanied by two other smaller lobes growing sideways) [38]. Moreover, enhanced growth of mode $4k$ may lead to finger tip quadrifurcation [39], etc. Of course, the nonlinear coupling among these modes could also lead to a multitude of other morphological structures. In this fashion, our perturbative mode-coupling scheme can be very helpful in the search for still unexplored pattern-forming shapes that might arise under the presence of magnetoelastic effects in horizontal, rectangular Hele-Shaw cells.

To study the development of interfacial patterns in our problem, we rewrite Eq. (14) for the complex mode amplitudes ζ_k in terms of the real-valued cosine amplitudes $a_k = \zeta_k + \zeta_{-k}$ and write the perturbed elastic interface as

$$\zeta(x,t) = a_k(t)\cos(kx) \; + \; a_{2k}(t)\cos(2kx) + a_{3k}(t)\cos(3kx) \; + \; a_{4k}(t)\cos(4kx). \tag{27}$$

The time-dependent mode amplitudes a_k, a_{2k}, a_{3k}, and a_{4k} are obtained by numerically solving a considerably lengthy set of somewhat convoluted, coupled differential equations, composed of Eqs. (14)–(26).

Before examining the finger-shape behaviors at third order, we make a few important remarks. Notice that the equation of motion of our problem [Eq. (14)] involves the dimensionless parameters: N_B, A, U, λ, and C. However, for the sake of simplicity, and without loss of generality, throughout this work we concentrate our attention on examining the influence of the magnetoelastic number N_B and of the bending rigidity parameter C on the formation of the fingered patterns. This is done for the following reasons: first, as mentioned previously in this work, to keep a connection with the most traditional circumstances in horizontal, rectangular Hele-Shaw flows [1,3], we choose to focus on the popular situation of maximum viscosity contrast $A = 1$. In addition, without affecting the generality of our theoretical analysis, we take a representative value of the characteristic velocity $U = 2$. In the linear stability (Sec. III A), we have seen that U has a destabilizing role, and this is essentially its role at third order. In any case, we have verified that our results are not unexpectedly changed if other allowed values of U are used. Finally, as long as elastic effects are concerned, we consider a fixed value of the characteristic radius ($\lambda = 1$) and alter elastic effects by varying the bending rigidity fraction parameter C, where $0 \leqslant C < 1$. So, without affecting the validity and relevance of our theoretical analysis, in the remainder of this work, the understanding of the most relevant physical aspects of our problem will be described by the action of only two parameters: N_B and C.

We begin our discussion by analyzing Fig. 3, which presents a representative set of weakly nonlinear, third-order patterns. Since the central goal of our study is to reveal the effects of N_B and C on the morphology of the magnetoelastic fingering patterns, the results presented in Fig. 3 focus on illustrating the most characteristic aspects of the fingers for different combinations of these parameters. Therefore, in Fig. 3(a) $C = 0$ and $N_B = 0$, in Fig. 3(b) $C = 0.99$ and $N_B = 0$, while in Fig. 3(c) these two patterns are overlaid. Likewise, in Fig. 3(d) $C = 0$ and $N_B = 4$, in Fig. 3(e) $C = 0.99$ and $N_B = 4$, while in Fig. 3(f) these interfaces are superimposed. The values of the fastest

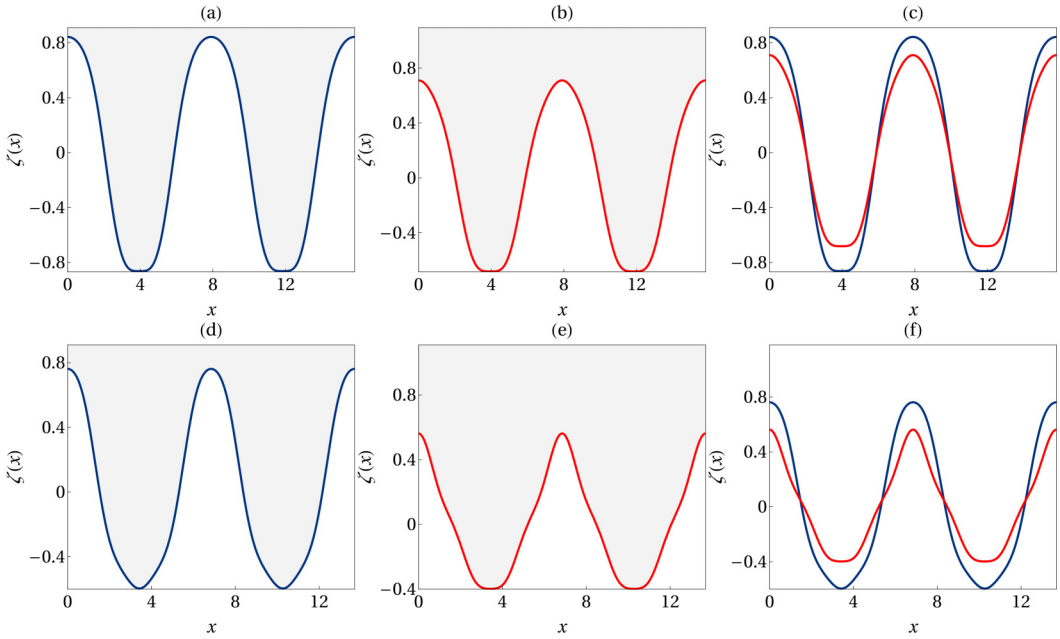

FIG. 3. Representative weakly nonlinear, third-order, magnetoelastic interfacial patterns for (a) $C = 0$, $N_B = 0$; (b) $C = 0.99$, $N_B = 0$; (d) $C = 0$, $N_B = 4$; (e) $C = 0.99$, $N_B = 4$. In (c) the patterns depicted in (a) and (b) are overlaid. Likewise, in (f) the patterns illustrated in (d) and (e) are superimposed.

growing modes used in Figs. 3(a) and 3(b) is $k^* = 0.795$, whereas in Figs. 3(c) and 3(d) is $k^* = 0.917$. Moreover, we utilize the initial conditions: $a_k(0) = 10^{-5}$, and $a_{2k}(0) = a_{3k}(0) = a_{4k}(0) = 0$. The initial conditions are set in such a way that we can ensure that the initial growth of the modes $2k$, $3k$, and $4k$ are driven solely by nonlinear effects. This is done to make sure that the interfacial behaviors we observe in this work are spontaneously induced by the weakly nonlinear dynamics, and not by artificially imposing large initial amplitudes for the harmonic modes.

It should be noted that while plotting the interfacial patterns shown in Fig. 3, and in subsequent figures in this work, we stop the time evolution as soon as the base of the fingers (or the valleys that separate an array of fingers) start to present small-amplitude oscillations. These oscillations definitely do not appear in real experiments of (nonelastic) ferrofluid peak formation induced by in-plane magnetic fields in rectangular Hele-Shaw cells [14,16,17]. They are also not seen in numerical simulations of the system [15,21]. Nevertheless, some perturbative studies [18,19] that try to model these experiments sometimes reveal the development of such small oscillations at the finger bases or valleys of the fingering structures (see, for instance, Figs. 4 and 5 in Ref. [18], and Fig. 1(b) in Ref. [19]). It turns out that these oscillations are an artifact of these types of perturbative descriptions, when one goes beyond the validity of the models used (for example, when the time considered is too long). Therefore, in this work we adopt the longest time before the appearance of such nonphysical small oscillations as the upper-bound time ($t_{\max}$) for the validity of our perturbative third-order theoretical description. Having said this, the times $t_{\max}$ used in Fig. 3 are (a) 8.956, (b) 6.450, (d) 8.770, and (d) 6.157.

We initiate our discussion of Fig. 3 by examining the situation when no external magnetic field is applied ($N_B = 0$). The fingering pattern displayed in Fig. 3(a) for $C = 0$ corresponds to the case of largest resistance of the elastic interface to disturbances; i.e., it is the case of maximum rigidity. Under such circumstances, the result is the formation of a finger having a fairly rounded tip. On the other hand, in Fig. 3(b) we have a large value of the rigidity fraction ($C = 0.99$), meaning that the elastic interface is much more flexible. Consequently, a significantly different

pattern is formed, leading to the development of a finger that is sharper at the finger tip than the one obtained in Fig. 3(a). Note that the finger depicted in Fig. 3(b) is different from the classical Saffman-Taylor finger [1] where the interface is not elastic and surface tension is present. The increased tendency toward the appearance of sharper tips for larger values of C can be understood as a result of the curvature-dependent bending rigidity model [Eq. (8)]: flow-induced interfacial deformations decrease the rigidity, allowing the elastic interface to be deformed more easily as the local interfacial curvature increases. The distinctions between the patterns for $C = 0$ and $C = 0.99$ can be easily verified in Fig. 3(c). It is worthwhile noting that the types of finger morphologies portrayed in Figs. 3(a)–3(c), obtained in the absence of an applied magnetic field ($N_B = 0$), has no parallel with shapes found in the equivalent magnetoelastic problem in a vertical Hele-Shaw cell studied in Ref. [22]. After all, if N_B is set to zero in the circumstances considered in Ref. [22], the elastic ferrofluid interface would be flat and stable.

Now we turn our attention to the cases in which an external magnetic field is applied ($N_B = 4$), acting concurrently with the elastic effects of the interface. By inspecting Fig. 3(d) for $C = 0$, we see that despite the large rigidity of the elastic interface, the action of the magnetic field produces fingers that are considerably narrow along their bodies, as well as significantly sharper near the tips than the corresponding structure obtained when $N_B = 0$ [Fig. 3(a)]. Observe that the narrow and sharp central finger displayed in Fig. 3(d) has some similarities with the equivalent structure obtained experimentally in Ref. [14] for the nonelastic, ferrofluid flow case (their Fig. 7). Yet another type of finger shape is unveiled in Fig. 3(e) when $C = 0.99$ and $N_B = 4$. The presence of the magnetic field, and the reduced rigidity of the interface lead to a finger that is quite sharp at the finger tip, exhibiting a characteristic peak shape. The differences in shape obtained when C changes from 0 to 0.99 when $N_B = 4$ are graphed in Fig. 3(f). Additionally, by contrasting Figs. 3(b) and 3(e) it is also clear that the action of the applied magnetic field exacerbates the existing tendency to form sharp fingers induced by the decreased rigidity conditions of the elastic interface. The third-order results shown in Fig. 3 demonstrate that our willingness to go the such a high-order perturbation level has been rewarded by the appearance of interesting pattern-forming structures.

Figure 3 offers a representative compilation of interface shapes for our magnetoelastic fingering problem in horizontal, rectangular Hele-Shaw geometry, for two extreme values of the bending rigidity fraction ($C = 0$ and $C = 0.99$) and for a characteristic magnetoelastic number ($N_B = 4$). To better characterize the impact of the parameters N_B and C on the morphologies of the fingers for a whole range of values of C and also for other typical values of N_B, in Fig. 4 we plot the finger tip curvatures κ as a function of C ($0 \leqslant C \leqslant 0.99$) at times $t = t_{\max}$, for $N_B = 0$, 0.2, 2, and 4. The rest of the parameters (A, U, and λ) are those utilized in Fig. 3. But, as expected, the values for k^*, and $t_{\max}$ vary from point to point.

Figure 4 unfolds a rich spectrum of possible finger tip behaviors as N_B and C are varied. For example, when $N_B = 0$ we can see the finger tip curvature modestly decreases from $C = 0$ up to $C \approx 0.1$ and then slowly increases as $C \to 0.99$. However, already for small nonzero values of the magnetoelastic number ($N_B = 0.2$) one can verify that the sequence of events change considerably: initially, for small C, κ drops to a minimum and then rises monotonically as C is increased. This scenario changes even more radically for larger values of N_B. For example, when $N_B = 2$, the initial responses are qualitatively similar to the case $N_B = 0.2$, but after reaching a certain value of C ($C \approx 0.68$), the tip curvature abruptly increases, reaches a maximum, and then falls off. A somewhat similar trend is followed by κ when $N_B = 4$. The general qualitative behavior of κ for higher values of the magnetoelastic number takes similar steps as those observed for $N_B = 4$.

Figure 4 makes clear that, by varying the values of C and N_B, one can identify a variety of interesting dynamical behaviors and possible morphological responses for the magnetoelastic patterns. However, it is also evident that the interplay of C and N_B in determining the finger tip curvature, and consequently the overall finger shape, is not at all trivial. This complex scenario arises due to the fact that here, not only the bending rigidity $\nu(\kappa)$, but also the demagnetizing field effects, are dependent on the shape of the interface. In order to illustrate a representative example of the various pattern-forming structures that may arise within a plethora of possibilities offered in

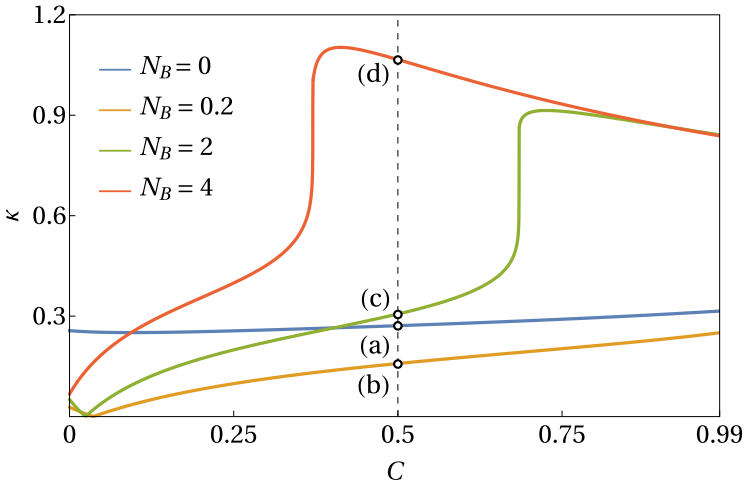

FIG. 4. Behavior of the curvature of the finger tip κ as the bending rigidity parameter C is varied from 0 to 0.99 at times $t = t_{\max}$, for four values of the magnetoelastic number N_B: 0, 0.2, 2, and 4. The weakly nonlinear, third-order magnetoelastic shapes corresponding to points (a)–(d) given by the intersection of the vertical dashed line at $C = 0.5$ with the various curves are presented in Fig. 5.

Fig. 4, in Fig. 5 we portray the interfacial patterns that arise at points (a), (b), (c), and (d) indicated in Fig. 4. These points are given by the intersection of the vertical dashed line with the curves for κ for an intermediate value of the bending rigidity fraction ($C = 0.5$). Notice that the values of the wave numbers of maximum growth and the maximum possible times in these cases are the following: (a) $k^* = 0.795$, $t_{\max} = 8.822$; (b) $k^* = 0.801$, $t_{\max} = 8.685$; (c) $k^* = 0.857$, $t_{\max} = 7.474$; and (d) $k^* = 0.918$, $t_{\max} = 6.307$.

For point (a) [Fig. 5(a)], which is related to a situation for which $N_B = 0$, we have the formation of a traditional looking finger having a rounded tip. This structure is pretty similar to the one we have obtained in Fig. 3(a). Nonetheless, for point (b) [Fig. 5(b)], when the magnetoelastic number is increased to $N_B = 0.2$, we observe a remarkable feature at the finger tip: it acquires a straight front, perpendicular to the direction of motion. This is completely unlike the rounded tips of most conventional Saffman-Taylor fingers [1,3]. Interestingly, a similar type of flat tip fingered pattern was detected in the experiments of elastic fingering for nonmagnetic fluids in rectangular Hele-Shaw flow perform by Podgorski *et al.* [4]. The straight front finger illustrated in Fig. 5(b) is another example of finger morphology that has not been detected in Ref. [22]. Then, for point (c) [Fig. 5(c)], for an augmented value of the magnetoelastic number $N_B = 2$, the finger tip becomes rounded again, irrespective of the fact that N_B has been increased. Finally, for point (d) [Fig. 5(d)], for which $N_B = 4$, one encounters a finger having a very sharp tip, reminiscent of the finger shape found in Fig. 3(e). Other type of scenarios can be found if one chooses different values of C in Fig. 4. But the point here is that Figs. 3–5 already capture and illustrate well the basic types of magnetoelastic patterns one can get in horizontal, rectangular Hele-Shaw cells.

1. Nonelastic fingering patterns

In this section, we briefly discuss how the morphology of the typical magnetoelastic fingering patterns obtained in this study (where magnetic, elastic, and viscous effects compete) compare with the corresponding fingering structures studied experimentally in Ref. [14], where elastic effects are replaced by capillary effects in such a way that magnetic, surface tension, and viscous forces rival one another. To produce these nonelastic patterns, we had to derive the equivalent third-order

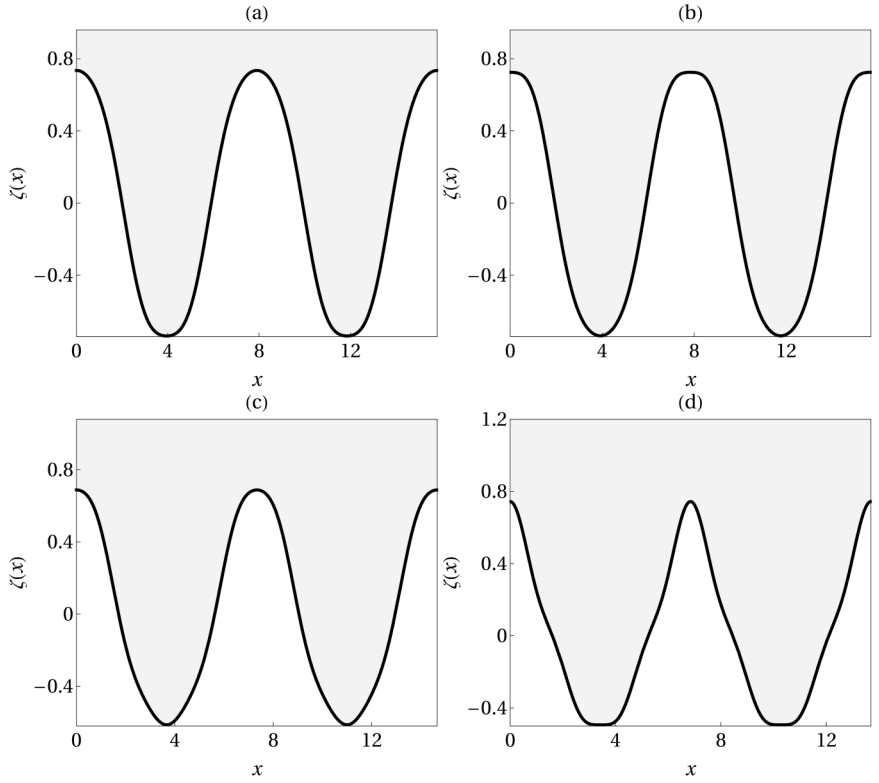

FIG. 5. Representative weakly nonlinear, third-order magnetoelastic patterns that arise at points (a)–(d) in Fig. 4.

mode-coupling equation for the nonelastic case (see the Appendix). Notice that the study of such types of nonelastic fingering patterns was not explored in Ref. [22].

Figure 6 depicts typical nonelastic viscous fingering counterparts of the magnetoelastic fingers illustrated in Figs. 3 and 5. Recall that the main difference between the two situations is that in Fig. 6 elastic effects are not present and on the interface there is a surface tension. Other than that,

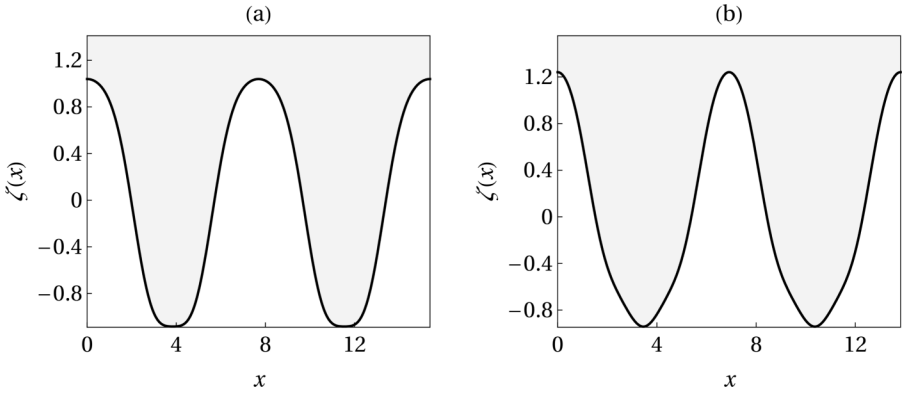

FIG. 6. Typical weakly nonlinear, third-order, *nonelastic* interfacial patterns for $\mathcal{U} = 2$ and (a) $\mathcal{N}_B = 0$, and (b) $\mathcal{N}_B = 0.1$.

the physical system is exactly the same: a fluid of negligible viscosity displaces a viscous ferrofluid in a horizontal, rectangular Hele-Shaw cell, under the presence of an in-plane, uniform magnetic field.

The nonelastic patterns are obtained by utilizing the same initial conditions and participating modes used in Figs. 3 and 5. Nevertheless, now we have new definitions for the relevant dimensionless parameters of the nonelastic system. In the nonelastic case we deal with a magnetic Bond number $\mathcal{N}_B$ and with a characteristic velocity parameter $\mathcal{U}$ (see the Appendix). The particular values of the parameters used Fig. 6 are such that they generate fastest growing modes similar to those produced in the corresponding magnetoelastic fingering cases. Naturally, to get the patterns shown in Fig. 6 we use the third-order mode-coupling differential equation [Eq. (14)] and its first-, second-, and third-order coefficients presented in the Appendix. The nonelastic patterns portrayed in Fig. 6 are obtained by setting $\mathcal{U} = 2$, when $\mathcal{N}_B = 0$ [Fig. 6(a)] and $\mathcal{N}_B = 0.1$ [Fig. 6(b)]. In addition, the values for the fastest growing modes and maximum allowed times used are (a) $k^* = 0.816$, $t_{\max} = 10.73$ and (b) $k^* = 0.909$, $t_{\max} = 9.44$.

As exemplified well in Fig. 6, in the nonelastic case we basically have the uprising of two types of patterns. As expected, in the absence of a applied external field [Fig. 6(a)] one gets a typical Saffman-Taylor-like finger, having a rounded tip. On the other hand, when the in-plane magnetic field is applied [Fig. 6(b)] we observe the formation of a different fingering structure, where the finger is much sharper near its tip, due to the action of the demagnetizing field effects. Moreover, the width of the finger illustrated in Fig. 6(b) varies more strongly along its length than in the zero applied field case shown in Fig. 6(a). It is reassuring to see that the third-order perturbative pattern presented in Fig. 6(b) captures the essential morphological features of the experimental pattern obtained by Pacitto *et al.*, as depicted in Fig. 7 of Ref. [14], and of the numerically simulated pattern shown in Fig. 3.26 of Ref. [15]. Despite this, it should be stressed that the representative nonelastic shapes plotted in Fig. 6 are indeed the only two basic pattern-forming structures we were able to get. This is in contrast with the richer magnetoelastic scenario exposed in Figs. 3–5, where a number of different patterns may arise by tuning C and N_B. This reinforces the relevance of studying magnetoelastic fingering in horizontal, rectangular Hele-Shaw cells.

IV. CONCLUSION

In this work we have provided a theoretical study of the magnetoelastic flow in a horizontal, rectangular Hele-Shaw cell. Our current third-order mode-coupling investigation expands our previous lower-order analyses for the development of magnetoelastic interfacial patterns in radial Hele-Shaw cell geometry [29,30] to the rectangular flow setup. In addition, it complements our recent study [22] where a similar problem has been examined in a vertical rectangular Hele-Shaw cell under the presence of gravity and without any external flow velocity. While in the traditional Saffman-Taylor situation in horizontal cells the interplay of viscous and surface tension forces generates a finger having a rounded tip, our third-order weakly nonlinear theory reveals the emergence of significantly different fingered structures that result from the competition of magnetic, elastic, and viscous effects.

At early stages, our linear stability analysis indicates that the applied magnetic field is destabilizing and competes with a stabilizing constant bending rigidity. We have found that at the linear level such an elastic effect acts similar to its surface tension counterpart in the classical Saffman-Taylor problem [see Eqs. (15) and (A2)]. No curvature-dependent bending rigidity contribution has been detected in the linear stage. In the weakly nonlinear, second-order regime, we have verified that the magnetic field favors the formation of fingers that are sharp at their tips. This particular second-order finger-tip-sharpening effect is due to the action of a magnetic traction contribution in the pressure jump boundary condition [Eq. (12)]. This magnetic term is maximized when the unit normal vector at the interface $\mathbf{n}$ is collinear to the applied field $\mathbf{H}_0$, so that once a finger protuberance is formed at the tip, the growing peak tends to become sharper. No influence of the curvature-dependent bending rigidity has been found at second order.

Nevertheless, at third order a much more interesting pattern-forming scenario is unveiled, where curvature-dependent bending rigidity, magnetic, and viscous effects rival each other. By tuning two controlling dimensionless parameters, namely, the magnetoelastic number N_B and the bending rigidity fraction C, we have obtained a representative collection of fingered structures, revealing the formation of patterns having different shapes, where their finger tip may vary from flat, rounded, or sharp, to very pointy, as the values of N_B and C are changed. Our third-order theoretical results indicate that these magnetoelastic patterns are not only significantly distinct from the usual nonmagnetic Saffman-Taylor finger [1], but also differ from the nonelastic finger generated when a ferrofluid is pushed by a nonmagnetic fluid under the action of an applied, in-plane magnetic field [14]. Our theoretical results highlight the effect of replacing surface tension by bending rigidity in the instabilities observed in horizontal, rectangular Hele-Shaw flows involving nonmagnetic, as well as magnetic fluids.

As commented earlier in this work, our current magnetoelastic study should not be viewed simply as a complex theoretical but somewhat hypothetical exercise. In principle, experimental realizations are possible and should be pursued. Moreover, the development of fully nonlinear numerical simulations for the magnetoelastic problem reported here in rectangular Hele-Shaw cell geometry could also be a possible extension of this perturbative work, in the same spirit of the extensive numerical investigation performed in Ref. [9] for the nonmagnetic elastic fingering problem in radial geometry. Hopefully, this work will instigate further theoretical and experimental studies on this pattern formation research topic.

ACKNOWLEDGMENTS

J.A.M. thanks CNPq (Conselho Nacional de Desenvolvimento Científico e Tecnológico) for financial support under Grant No. 305140/2019-1. We gratefully acknowledge useful discussions with T. Podgorski.

APPENDIX: MODE-COUPLING DIFFERENTIAL EQUATION TERMS FOR THE NONELASTIC FINGERING PROBLEM

This Appendix presents the expressions for the first-, second-, and third-order coefficients which appear in the third-order mode-coupling differential equation for the *nonelastic* fingering situation. Under nonelastic circumstances, elastic effects are absent, and magnetic, surface tension, and viscous forces compete. It is worthwhile to note that such a nonelastic third-order mode-coupling equation is formally identical to Eq. (14) but has some different coefficients. In the nonelastic case, the pressure boundary condition corresponding to our Eq. (12) is much simpler and given by [1,3,5,33]

$$(p_1 - p_2)|_{y=\zeta} = -\sigma\kappa - \tfrac{1}{2}\mu_0(\mathbf{M}\cdot\mathbf{n})^2, \tag{A1}$$

where σ is the surface tension between the fluids. Performing our weakly nonlinear analysis in the same away as we did in Sec. II for the magnetoelastic fingering case, we obtain the nonelastic analogues of Eqs. (15)-(26), namely,

$$\Lambda(k) = |k|[\mathcal{N}_B W_1(k) + A\mathcal{U} - k^2], \tag{A2}$$

$$J(k, p, q) = -\tfrac{3}{2}|k|p^2 q(k - p - q), \tag{A3}$$

where

$$\mathcal{N}_B = \frac{\mu_0 M^2 b}{4\pi\sigma} \tag{A4}$$

is the magnetic Bond number which relates magnetic to surface tensions effects, and

$$\mathcal{U} = \frac{12(\eta_2 + \eta_1)v_\infty}{\sigma} \tag{A5}$$

is a characteristic velocity parameter that measures the relative strength between viscous and surface tension forces.

We stress that all the equations presented in this Appendix are made dimensionless by using the following rescaling: lengths are rescaled by b as in our current magnetoelastic problem, but velocities are rescaled by $\sigma/[12(\eta_1 + \eta_2)]$. Note that the functions $G(k, q)$, $H(k, p, q)$, $I(k, p, q)$ and the magnetic integrals $W_1(k)$, $W_2(k)$, and $W_3(k)$ are the same as the ones obtained in the magnetoelastic case in Sec. II. In addition, the functions $F(k, q)$ and $K(k, p, q)$ for the nonelastic case can be obtained from their magnetoelastic counterparts [Eqs. (19) and (24), respectively] simply by replacing N_B by $\mathcal{N}_B$.

[1] P. G. Saffman and G. I. Taylor, The penetration of a fluid into a porous medium or Hele-Shaw cell containing a more viscous liquid, Proc. R. Soc. London A **245**, 312 (1958).

[2] L. Paterson, Radial fingering in a Hele-Shaw cell, J. Fluid Mech. **113**, 513 (1981).

[3] G. M. Homsy, Viscous fingering in porous media, Annu. Rev. Fluid Mech. **19**, 271 (1987); K. V. McCloud and J. V. Maher, Experimental perturbations to Saffman-Taylor flow, Phys. Rep. **260**, 139 (1995); J. Casademunt, Viscous fingering as a paradigm of interfacial pattern formation: Recent results and new challenges, Chaos **14**, 809 (2004).

[4] T. Podgorski, M. C. Sostarecz, S. Zorman, and A. Belmonte, Fingering instabilities of a reactive micellar interface, Phys. Rev. E **76**, 016202 (2007).

[5] R. E. Rosensweig, *Ferrohydrodynamics* (Cambridge University Press, Cambridge, 1985).

[6] E. Blums, A. Cebers, and M. M. Maiorov, *Magnetic Fluids* (de Gruyter, New York, 1997).

[7] A. He, J. S. Lowengrub, and A. Belmonte, Modeling an elastic fingering instability in a reactive Hele-Shaw flow, SIAM J. Appl. Math. **72**, 842 (2012).

[8] G. D. Carvalho, J. A. Miranda, and H. Gadêlha, Interfacial elastic fingering in Hele-Shaw cells: A weakly nonlinear study, Phys. Rev. E **88**, 053006 (2013).

[9] M. Zhao, A. Belmonte, S. Li, X. Li, and J. S. Lowengrub, Nonlinear simulations of elastic fingering in a Hele-Shaw cell, J. Comput. Appl. Math. **307**, 394 (2016).

[10] J.-C. Bacri, R. Perzynski, and D. Salin, Magnetic liquids, Endeavour **12**, 76 (1988).

[11] C. Rinaldi, A. Chaves, S. Elborai, X. He, and M. Zahn, Magnetic fluid rheology and flows, Curr. Opin. Colloid Interface Sci. **10**, 141 (2005).

[12] D. Andelman and R. E. Rosensweig, Modulated phases: Review and recent results, J. Phys. Chem. B **113**, 3785 (2009).

[13] J.-C. Bacri and F. Elias, in *Morphogenesis: Origins of Patterns and Shapes*, edited by P. Bourgine and A. Lesne, (Springer, New York, 2011).

[14] G. Pacitto, C. Flament, and J.-C. Bacri, Viscous fingering in a magnetic fluid. II. Linear HeleâShaw flow, Phys. Fluids **13**, 3196 (2001).

[15] M. Igonin, Hydrodynamic instabilities of miscible and immiscible magnetic fluids in a Hele-Shaw cell, Ph.D. thesis, D. Diderot University Paris 7, (2004).

[16] J.-C. Bacri and D. Salin, First-order transition in the instability of a magnetic fluid interface, J. Phys. Lett. **45**, 559 (1984).

[17] C. Flament, S. Lacis, J.-C. Bacri, A. Cebers, S. Neveu, and R. Perzynski, Measurements of ferrofluid surface tension in confined geometry, Phys. Rev. E **53**, 4801 (1996).

[18] A. Engel, H. Langer, and V. Chetverikov, Non-linear analysis of the surface profile resulting from the one-dimensional Rosensweig instability, J. Magn. Magn. Mater. **195**, 212 (1999).

[19] A. Engel, A. Lange, H. Langer, T. Mahr, and V. Chetverikov, A single peak of the Rosensweig instability, J. Magn. Magn. Mater. **201**, 310 (1999).

[20] S. A. Lira and J. A. Miranda, Weakly nonlinear study of normal-field instability in confined ferrofluids, Phys. Rev. E **84**, 016303 (2011).
[21] R. H. Nochetto, A. J. Salgado, and I. Tomas, A diffuse interface model for two-phase ferrofluid flows, Comput. Methods Appl. Mech. Eng. **309**, 497 (2016).
[22] I. M. Coutinho and J. A. Miranda, Peak instability in an elastic interface ferrofluid, Phys. Fluids **32**, 052104 (2020).
[23] J.-C. Bacri, V. Cabuil, A. Cebers, C. Menager, and R. Perzynski, Flattening of ferro-vesicle undulations under a magnetic field, Europhys. Lett. **33**, 235 (1996).
[24] C. Wischnewski and J. Kierfeld, Spheroidal and conical shapes of ferrofluid-filled capsules in magnetic fields, Phys. Rev. Fluids **3**, 043603 (2018).
[25] S. Neveu-Prin, V. Cabuil, R. Massart, P. Escaffre, and J. Dussaud, Encapsulation of magnetic fluids, J. Magn. Magn. Mater. **122**, 42 (1993).
[26] O. Sandre, C. Ménager, J. Prost, V. Cabuil, J.-C. Bacri, and A. Cebers, Shape transitions of giant liposomes induced by an anisotropic spontaneous curvature, Phys. Rev. E **62**, 3865 (2000).
[27] F. Serwane, A. Mongera, P. Rowghanian, D. A. Kealhofer, A. A. Lucio, Z. M. Hockenbery, and O. Campàs, In vivo quantification of spatially-varying mechanical properties in developing tissues, Nat. Methods **14**, 181 (2017).
[28] C. Wilhelm, F. Gazeau, and J.-C. Bacri, Magnetic micromanipulation in the living cell, Europhys. News **36**, 89 (2005) and references therein.
[29] P. O. S. Livera and J. A. Miranda, Magnetoelastic pattern formation in field-responsive fluids, Phys. Rev. Fluids **5**, 014006 (2020).
[30] P. H. A. Anjos, G. D. Carvalho, S. A. Lira, and J. A. Miranda, Wrinkling and folding patterns in a confined ferrofluid droplet with an elastic interface, Phys. Rev. E **99**, 022608 (2019).
[31] Thomas Podgorski (private communication).
[32] G. Pacitto, C. Flament, J.-C. Bacri, and M. Widom, Rayleigh-Taylor instability with magnetic fluids: Experiment and theory, Phys. Rev. E **62**, 7941 (2000).
[33] G. K. Batchelor, *An Introduction to Fluid Dynamics* (Cambridge University Press, Cambridge, 2000).
[34] C. Duprat and H. Stone (Eds), *Fluid-Structure Interactions in Low-Reynolds-Number Flows* (RSC, Cambridge, 2016).
[35] J. A. Miranda and M. Widom, Weakly nonlinear investigation of the Saffman-Taylor problem in a rectangular Hele-Shaw cell, Int. J. Mod. Phys. B **12**, 931 (1998).
[36] P. H. A. Anjos, S. A. Lira, and J. A. Miranda, Fingering patterns in magnetic fluids: Perturbative solutions and the stability of exact stationary shapes, Phys. Rev. Fluids **3**, 044002 (2018).
[37] J. A. Miranda and M. Widom, Radial fingering in a Hele-Shaw cell: A weakly nonlinear analysis, Physica D **120**, 315 (1998).
[38] R. Brandão, J. V. Fontana, and J. A. Miranda, Interfacial pattern formation in confined power-law fluids, Phys. Rev. E **90**, 013013 (2014).
[39] P. H. A. Anjos, E. O. Dias, and J. A. Miranda, Radial fingering under arbitrary viscosity and density ratios, Phys. Rev. Fluids **2**, 084004 (2017).